Optics Letters

Frequency comb dynamics of a 1.3 μm hybrid-silicon quantum dot semiconductor laser with optical injection

Bozhang Dong,[1,*] Heming Huang,[1] Jianan Duan,[1] Geza Kurczveil,[2] Di Liang,[2] Raymond G. Beausoleil,[2] and Frédéric Grillot[1,3]

[1]LTCI, Télécom Paris, Institut Polytechnique de Paris, 46 rue Barrault, 75013 Paris, France
[2]Hewlett Packard Labs, 1501 Page Mill Road, Palo Alto, California 94304, USA
[3]Center for High Technology Materials, University of New-Mexico, 1313 Goddard St. SE, Albuquerque, New Mexico 87106, USA
*Corresponding author: bozhang.dong@telecom-paris.fr

Received 23 September 2019; revised 26 October 2019; accepted 27 October 2019; posted 28 October 2019 (Doc. ID 378002); published 27 November 2019

This work reports on the influence of bias voltage applied on a saturable absorber (SA) on a subthreshold linewidth enhancement factor (LEF) in hybrid-silicon quantum dot optical frequency comb lasers. Results show that the reverse bias voltage on SA contributes to enlarge the LEF and improve the comb dynamics. Optical injection is also found to be able to improve the comb spectrum in terms of 3 dB bandwidth and its flatness. Such novel findings are promising for the development of high-speed dense wavelength-division multiplexing photonic integrated circuits in optical interconnects and datacom applications.

https://doi.org/10.1364/OL.44.005755

Wavelength-division multiplexing (WDM) solutions can be strongly supported by a variety of photonic integrated technologies that can be reused, as what was done in the telecommunication industry in using the vast amount of bandwidth offered by optical fibers, which contributed to enhance the data transmission. Therefore, the largest future cost reduction due to integration will then likely be enjoyed by more feature-rich blocks such as WDM versus a single-wavelength interface [1]. The realization of WDM functions is mainly based on multiple single-wavelength laser sources; however, the massive laser bar could be a disadvantage in several applications such as photonic integrated circuits (PICs). Optical frequency combs (OFCs) are thus a competitive candidate for WDM, considering that the past laser bar could be easily replaced by a single laser. Various researches on OFCs were deployed in the past decade for optical communications, in particular with quantum dot (QD) lasers, which were found to be efficient comb light sources owing to their very large gain bandwidth [2] as well as their narrow linewidth [2,3], low relative intensity noise [4], and higher resistance against external reflections [5,6] and temperature [7]. With the view of developing low-cost and energy-efficient integrated photonic components for PIC technologies, hybrid semiconductor comb lasers fabricated on silicon substrate have already shown high transmission efficiency [8]. Further improvements need to be carefully taken into account so as to obtain high performance OFCs with much larger bandwidth and optimal comb flatness. To this end, various techniques such as phase modulation [9], mode locking [10,11], and optical injection locking (OIL) [12,13] have been deployed. In this Letter, we go a step beyond by investigating the effects of the linewidth enhancement factor (LEF) and the optical injection (OI) on the comb performance of hybrid-silicon QD-OFCs. The former is known to be a key parameter in semiconductor lasers, hence influencing the spectral linewidth and the frequency chirp under direct modulation [14]. On the other hand, OI was proved to be an efficient way of improving the performance of semiconductor lasers such as the modulation bandwidth, the frequency chirp (as well as the intensity noise), and the transmission efficiency [15–17]. In this Letter, it is also shown that the frequency comb dynamics are stimulated at larger LEFs, whereas the OI can further improve both the bandwidth and the flatness of the entire comb spectrum. To do so, we report on the saturable absorber (SA) voltage dependence of the LEFs extracted from two hybrid-silicon QD-OFCs (named $L1$ and $L2$) and having the same free spectral range (FSR). The values of the LEFs are found to increase with the SA reverse voltage, which is in favor of better comb dynamics through increasing the single-mode suppression ratio (SMSR) of the comb lines. Last but not the least, the observed enhancement of both the bandwidth and the flatness of the entire comb spectrum proves that the OI technique is also strongly beneficial for improving the OFC dynamics.

Figure 1 depicts the schematic diagram of the hybrid-silicon QD-OFCs $L1$, and the full laser epitaxial structure can be found elsewhere [8]. Device $L1$ consists of a 2.3-mm-long internal cavity, which leads to 17 GHz FSR. A 1200-μm-long semiconductor optical amplifier (SOA) with a 120-μm-long SA at the center was then bonded on the laser cavity, with

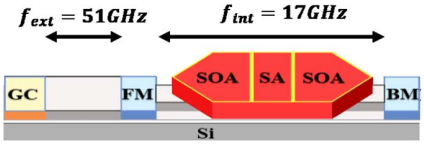

Fig. 1. Schematic diagram of the hybrid-silicon QD-OFCs *L*1. SOA, semiconductor optical amplifier; SA, saturable absorber; BM, back mirror; FM, front mirror; GC, grating coupler.

the front mirror (FM) and back mirror (BM) at ∼50% and ∼100% power reflectivities placed at both sides. The 0.75-mm-long (51 GHz) external cavity placed outside the laser cavity is then applied to get a 102 GHz FSR on frequency comb behavior. To do so, the SA at the center contributes at first to suppress every even mode of the laser cavity, thus changing the FSR from 17 to 34 GHz; then, the 51 GHz external cavity would only transmit every third mode of the 34 GHz FSR, and eventually ensures that the channel spacing of the comb laser is equal to 102 GHz (sixth harmonic of 17 GHz). The light would finally be coupled out by a ∼10% coupling efficiency grating coupler (GC). The comb dynamics are observed by varying the reverse voltage applied on the SA, whereas the mode converters are applied to transfer the optical mode between the active hybrid waveguide and the passive Si waveguide. Compared to *L*1, the differences in *L*2 structure are that it has not only a wider silicon waveguide of 0.85 μm (compared to 0.68 μm on device *L*1) but also a shorter SA of 60 μm. As those features may eventually cause a degradation in the OFC performance, the experimental study depicted hereinafter is mainly performed with device *L*1. In what follows, measurements are all conducted at room temperature (293 K).

Figure 2 depicts a mapping of the coupled power of *L*1 for different reverse voltages on SA and bias current conditions. The evolution of the threshold current I_{th} marked by the green dashed line is found to slightly increase from 32 to 38 mA as the reverse voltage is varied from 0 V to −6 V. At the same time, the coupled output power also decreases at higher reverse voltages. Such phenomenon, similar to that observed in mode-locked QD lasers on silicon [18], is due to the higher internal loss caused from the larger absorption in the SA. Let us note that the coupled power remains pretty low due to the loss induced by the vertical grating and the difficulty to monitor

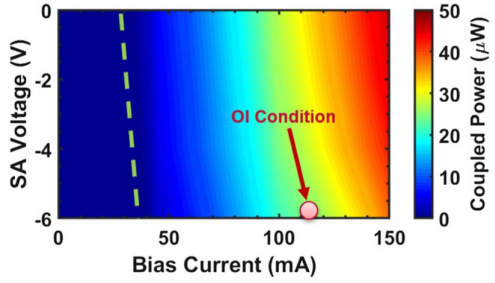

Fig. 2. Mapping of the coupled power (QD-OFCs *L*1) under different reverse voltages on SA and bias current conditions. The green dashed line represents the evolution of the laser threshold with the reverse voltage. The red bullet corresponds to the device operation conditions applied in the optical injection (OI), which is introduced in this Letter hereafter.

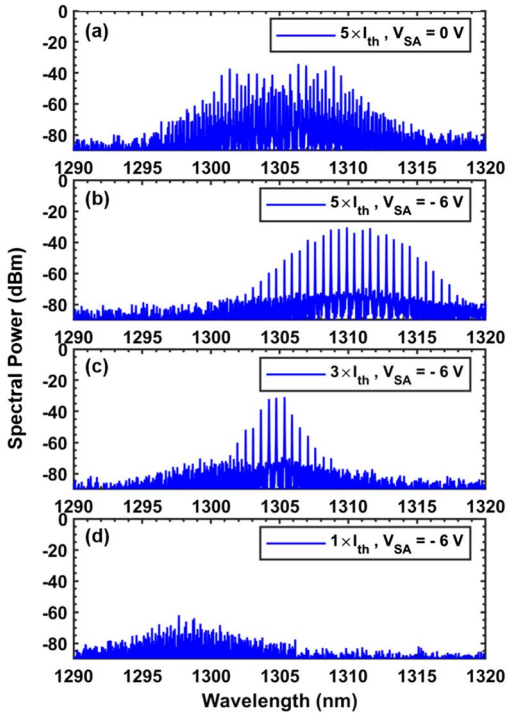

Fig. 3. Optical spectrum of QD-OFCs *L*1 at (a) $5 \times I_{th}$ without biasing SA and evolution of the combs forms of QD-OFCs *L*1 under bias voltage at −6 V on SA, with bias current at (b) $5 \times I_{th}$, at (c) $3 \times I_{th}$, and at (d) $1 \times I_{th}$.

the coupling during the whole experiment. A similar trend could also be observed on device L2 (not shown here).

Then, the effects of SA reverse voltage and bias current from the gain section on the comb dynamics are shown in Fig. 3 (device QD-OFCs *L*1). As aforementioned, the contribution of the SA on the occurrence of the comb dynamics can be clearly seen. Without biasing the SA, no comb spectrum is observed [Fig. 3(a)], whereas under a reverse voltage of −6 V, the laser exhibits a clear comb spectrum [Fig. 3(b)] at $5 \times I_{th}$. On the other hand, frequency comb behavior appears when the SA is properly biased, and the central wavelength redshift results from the increased internal loss introduced by absorption effect from SA as well. Assuming the best comb performance with −6 V reverse voltage, the influence of the bias current on the combs dynamics is now displayed in Figs. 3(b)–3(d). The increase of the bias current from $1 \times I_{th}$ to $5 \times I_{th}$ leads to a shift of the central frequency comb from 1298 to 1312 nm. This redshift of the comb position with the bias current is due to thermal effects. Moreover, it should be noticed that both the bandwidth and the flatness of the comb spectrum are also enhanced with the bias current. At $3 \times I_{th}$, the comb spectrum exhibits 12 lines above noise floor and three lines within 3 dB bandwidth [Fig. 3(c)] against 26 and eight, respectively, when the bias current increases to $5 \times I_{th}$ [Fig. 3(b)]. In general, comb dynamics are usually explained through the four-wave mixing (FWM) effect that is ruled out by the LEF [19]. In particular, both the sign and amplitude of the LEF associated with the different individual processes determine how the corresponding third-order susceptibilities contributions add up [20]. By the way, with the devices under study, a continuous-wave (CW) output, containing no pulses, is

preferred for WDM applications, as such devices are likely to have better reliability from the lower instantaneous power. In addition, the high instantaneous power of a temporally mode-locked laser is likely to trigger unwanted thermal nonlinearities [21] in the microring modulator array, which would degrade the signal being transmitted.

In this section, the extraction of the LEF is performed from the amplified spontaneous emission (ASE) [5,22]. In the experiment, we used a CW current source to get smooth optical modes, which would then be captured by a 20 pm high-resolution optical spectrum analyzer (OSA). Such operation ensures a better precision of the LEF extraction. The modal wavelength redshift above threshold caused by thermal effects is then totally subtracted from the wavelength blueshift below threshold, hence leading to an accurate extraction of the LEF from below to threshold. Let us note that the device temperature is carefully monitored and kept constant at room temperature (293 K) throughout the experiment.

Figure 4 displays the extracted LEF values (threshold) as the function of the reverse voltage on SA for devices $L1$ (blue) and $L2$ (red). In both cases, the LEFs are found to increase with the reverse voltage due to the decrease of the differential gain. For instance, it varies from 0.9 (without reverse voltage on SA) to 4.2 (−6 V on SA) for device $L1$. As for $L2$, a similar trend is observed except at the highest reverse voltage for which the LEF slightly drops down to 2.4. This last effect is attributed to the higher bias voltage applied on a shorter SA, causing more carriers being swept out and leading to a stronger reduction of the stimulated photon density. Together, these assumptions can explain the redecrease of the LEF at −6 V for device $L2$. Experiments depicted in Fig. 3 show that the comb dynamics is optimal when the LEF is larger. Indeed, the quadratic mean LEF calculated over the entire comb spectrum can be written as

$$(\overline{\alpha})_{\text{comb}} = \sqrt{\frac{1}{\Delta\nu}\int_{\text{comb}} \mathrm{d}\nu' \alpha^2(\nu')}, \tag{1}$$

with $\Delta\nu$ being the width of the comb spectrum while ν is the frequency of the radiation emitted by the laser. Therefore, assuming a QD as a two-level atomic system and that the entire gain media of the QD laser is composed of uniform QD with the same size, integration of Eq. (1) leads to $\Delta\nu = \Gamma\sqrt{3}(\overline{\alpha})_{\text{comb}}$, with Γ being the homogeneous broadening of the QD transition. Thus, this equation shows that a larger LEF is indeed more beneficial for improving the comb dynamics through FWM, as shown in Fig. 3 [23]. A larger LEF was also proved to enhance the mode-locking effect [24], which is in favor of improving the frequency comb dynamics. On the top of that, this equation shows that strengthening the spatial overlap among the dots and, hence, increasing the temperature-dependent homogeneous broadening can *a priori* contribute to further broaden the comb bandwidth [25]. However, this last statement has some limitations since the increase of the inhomogeneous broadening will not necessary lead to an unlimited increase of the frequency comb bandwidth. Indeed, for a larger gain linewidth, the FWM that is intended as the self-injection locking mechanism, in providing equally spaced and phase-locked modes, becomes less efficient because the dispersion for high-frequency active modes is bigger. Also, it is important to remember that the inhomogeneous broadening remains fundamentally an incoherent mechanism, thus potentially being more detrimental for a coherent phenomenon like frequency combs.

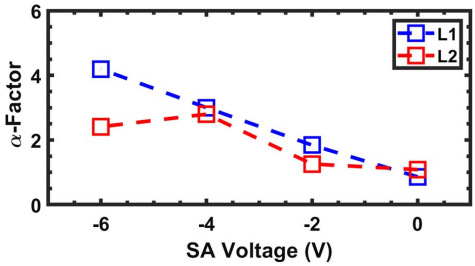

Fig. 4. Measured LEF at threshold as the function of the reverse voltage on SA for the QD-OFCs $L1$ (blue) and $L2$ (red).

As aforementioned, OIL has been broadly used in semiconductor lasers with the view to enhance the relaxation oscillations, or to reduce the relative intensity-to-noise, the nonlinear distortion, and most importantly the linewidth and frequency chirp [15]. In this Letter, we also investigated the effects of the OI as a way to process OFC by isolating and amplifying individual comb modes. A schematic illustrating the experimental setup is represented in Fig. 5. To this end, a master laser (ML) and a slave laser (SL) are involved. The ML is a single-mode laser with a narrow spectral linewidth, which is injected into the slave comb QD laser. The injection strength R_{inj}, in dBm, is calculated through the relationship

$$R_{\text{inj}} = P_{\text{ml}} - P_{\text{out}} + 2 \times (L_{\text{ext}} + L_{\text{fm}} + L_{\text{gc}}), \tag{2}$$

where P_{ml} is the injection power of ML, P_{out} is the free-space output power of the SL, L_{ext} is the one-way external cavity waveguide loss, and L_{fm} and L_{gc} are the FM and GC transmission loss, respectively. In the experiments, the values of L_{fm} and L_{gc} could be confirmed at −3 dB and −9 dB, respectively. By the way, the waveguide loss L_{ext} structures were not present on the mask, but it is estimated to be less than 2 dB/mm based on data from previous process runs. This should give an upper limit on the loss of the external cavity. Taking L_{ext} into account, the total loss could exceed −12 dB. Nevertheless, when it comes to the calculation of R_{inj}, such loss introduced by the external cavity should be doubled and eventually would exceed −24 dB.

Let us note that in these experiments, the frequency of the slave QD comb laser is not locked to that of the ML. Instead, a low OI strength is considered in order to optimize the combs dynamics. OI operation is served when the device $L1$ works at $3 \times I_{\text{th}}$ with −6 V applied on SA, and the R_{inj} could thus be estimated to be below −12 dB based on Eq. (2), as the P_{ml} and P_{out} are found to be 6 dBm and −6 dBm, respectively. Due to such low injection strength, the LEF is considered as not being affected by the injected field. In other words,

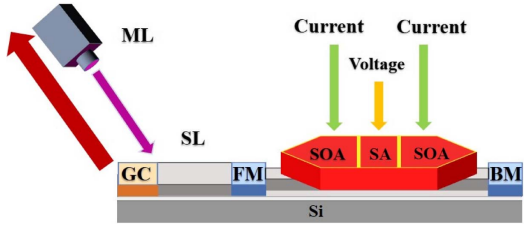

Fig. 5. Schematic illustrating optical injection operation. ML, master laser; SL, slave laser.

the LEF can be treated as a constant and does not impact the changes observed in the comb dynamics. Figure 6 unveils two types of OI-driven states on device $L1$ when operated at $3 \times I_{th}$ with −6 V reverse voltage on the SA. The free-running state (without OI) is shown in Fig. 6(a) as a reference. The inset of Fig. 6(a) highlights the injection wavelength of ML, seeing that the intramodal injection and intermodal injection are marked by a red arrow and a black arrow, respectively. Once OI intramodal injection is applied [injection wavelength at 1303.9 nm in this case, marked by a red arrow in Fig. 6(b)], a blueshift of the comb spectrum is observed. In this configuration, both the bandwidth and flatness of the comb spectrum can be regenerated compared to the free-running state. For instance, the full bandwidth of the comb laser broadens from 5.7 nm (11 lines above noise floor) to 10.7 nm (20 lines above noise floor), and its 3 dB bandwidth enlarges from 1.1 nm (three lines) to 4 nm (eight lines).

On the other hand, another OI-driven state can also be observed when intermodal OI is applied with an injection wavelength at 1305.2 nm, as marked by black arrow in Fig. 6(c). However, in this configuration, no obvious improvements of the comb dynamics is observed despite a slight redshift of the comb central wavelength. Therefore, intermodal injection does not allow us to improve the bandwidth nor the flatness of the entire comb spectrum. The reasons why two OI-driven states are unveiled between intra- and intermodal injections are uncertain yet; hence, corresponding studies would be investigated in further work.

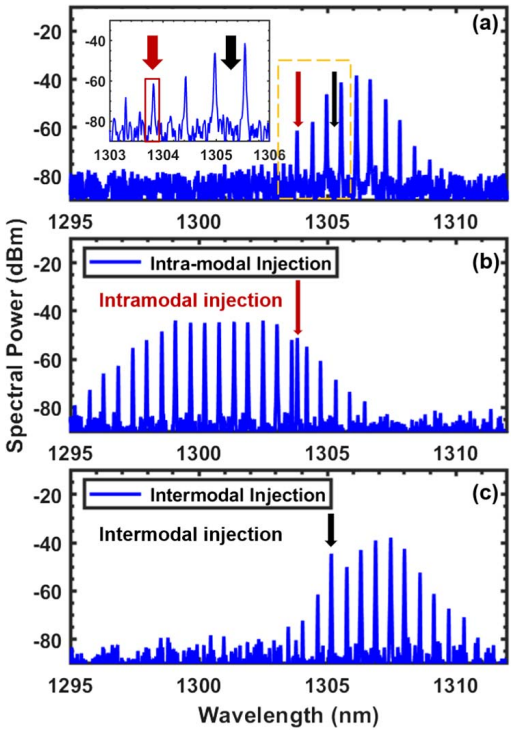

Fig. 6. (a) Optical spectra of $L1$ at free-running, and in the inset, the magnification of the yellow area in the figure. The intramodal injected wavelength (red arrow) and the intermodal injection wavelength (black arrow) of ML are highlighted. Optical spectra of $L1$ (b) under intramodal optical injection at 1303.9 nm (red arrow) and (c) under intermodal optical injection at 1305.2 nm (black arrow). Device is operated at $3 \times I_{th}$, and bias voltage applied on SA equals to −6 V.

To summarize, this work demonstrates the influence of the SA reverse voltage on subthreshold LEFs of hybrid-silicon QD-OFCs as well as the OI effect on enhancing the bandwidth and flatness of OFCs. A larger LEF was observed when higher reverse voltage was applied on SA, which contributes to enhance OFC performance. Intramodal OI was shown to improve the bandwidth and flatness of the comb spectrum. These novel findings are very encouraging for the future integrated technologies required for optical interconnects and datacom applications. Further work will now concentrate on the improvement of the QD devices as well as on the loss reduction in the experimental setup.

Disclosures. The authors declare no conflicts of interest.

REFERENCES

1. L. Han, B. P.-P. Kuo, N. Alic, and S. Radic, in *Optical Fiber Communications Conference Exhibits (OFC)* (2019), pp. 1–3.
2. Z. G. Lu, J. R. Liu, C. Y. Song, J. Weber, Y. Mao, S. D. Chang, H. P. Ding, P. J. Poole, P. J. Barrios, D. Poitras, S. Janz, and M. O'sullivan, Opt. Express **26**, 2160 (2018).
3. J. Duan, H. Huang, Z. G. Lu, P. J. Poole, C. Wang, and F. Grillot, Appl. Phys. Lett. **112**, 121102 (2018).
4. G. L. Wojcik, D. Yin, A. R. Kovsh, A. E. Gubenko, I. L. Krestnikov, S. S. Mikhrin, D. A. Livshits, D. A. Fattal, M. Fiorentino, and R. G. Beausoleil, Proc. SPIE **7230**, 72300M (2009).
5. J. Duan, H. Huang, B. Dong, D. Jung, J. C. Norman, J. E. Bowers, and F. Grillot, IEEE Photon. Technol. Lett. **31**, 345 (2019).
6. A. Liu, T. Komljenovic, M. Davenport, A. Gossard, and J. Bowers, Opt. Express **25**, 9535 (2017).
7. T. Kageyama, K. Nishi, M. Yamaguchi, R. Mochida, Y. Maeda, K. Takemasa, Y. Tanaka, T. Yamamoto, M. Sugawara, and Y. Arakawa, in *Conference on Lasers and Electro-Optics Europe and 12th European Quantum Electronics Conference (CLEO EUROPE/EQEC)* (2011).
8. G. Kurczveil, M. A. Seyedi, D. Liang, M. Fiorentino, and R. G. Beausoleil, IEEE Photon. Technol. Lett. **30**, 71 (2018).
9. V. R. Supradeepa and A. M. Weiner, Opt. Lett. **37**, 3066 (2012).
10. Z. G. Lu, J. R. Liu, P. J. Poole, S. Raymond, P. J. Barrios, D. Poitras, G. Pakulski, P. Grant, and D. Roy-Guay, Opt. Express **17**, 3066 (2009).
11. M. Yu, Y. Okawachi, A. G. Griffith, M. Lipson, and A. L. Gaeta, Optica **3**, 854 (2016).
12. E. Sooudi, C. de Dios, J. G. McInerney, G. Huyet, F. Lelarge, K. Merghem, R. Rosales, A. Martinez, A. Ramdane, and S. P. Hegarty, IEEE J. Sel. Top. Quantum Electron. **19**, 1101208 (2013).
13. E. Prior, C. De Dios, R. Criado, M. Ortsiefer, P. Meissner, and P. Acedo, Opt. Lett. **41**, 4083 (2016).
14. F. Grillot, B. Dagens, J. G. Provost, H. Su, and L. F. Lester, IEEE J. Quantum Electron. **44**, 946 (2008).
15. E. K. Lau, L. J. Wong, and M. C. Wu, IEEE J. Sel. Top. Quantum Electron. **15**, 618 (2009).
16. N. A. Naderi, M. Pochet, F. Grillot, N. B. Terry, V. Kovanis, and L. F. Lester, IEEE J. Sel. Top. Quantum Electron. **15**, 563 (2009).
17. J. Jignesh, A. Lowery, and B. Corcoran, Opt. Express **26**, 5733 (2018).
18. S. Liu, X. Wu, D. Jung, J. C. Norman, M. J. Kennedy, H. K. Tsang, A. C. Gossard, and J. E. Bowers, Optica **6**, 128 (2019).
19. T. Akiyama, H. Kuwatsuka, N. Hatori, Y. Nakata, H. Ebe, and M. Sugawara, IEEE Photon. Technol. Lett. **14**, 1139 (2002).
20. G. P. Agrawal, J. Opt. Soc. Am. B **5**, 147 (1988).
21. M. De Cea, A. H. Atabaki, and R. J. Ram, Opt. Express **27**, 24274 (2019).
22. M. Osinski and J. Buus, IEEE J. Quantum Electron. **23**, 9 (1987).
23. F. Cappelli, G. Villares, S. Riedi, and J. Faist, Optica **2**, 836 (2015).
24. M. Heuck, S. Blaaberg, and J. Mørk, Opt. Express **18**, 18003 (2010).
25. F. Grillot, K. Veselinov, M. Gioannini, I. Montrosset, J. Even, R. Piron, E. Homeyer, and S. Loualich, IEEE J. Quantum Electron. **45**, 872 (2009).